2026 IEEE International Conference on Robotics and Automation (ICRA 2026)
June 1-5, 2026. Vienna, Austria

FG-HOCBF: Safe Operation Area Extension and Obstacle Avoidance Direction Guidance for Surface Detection in Narrow Environments*

Yujie Li, Zhitao Gao, Chen Chen, Fangyu Peng, Yukui Zhang, Rong Yan, Xiaowei Tang, Wenke Zhou

***Abstract*— High-order control barrier functions (HOCBFs) that can achieve strict safety guarantees are widely used in robot safety control. However, robot obstacle avoidance in narrow environments with curved surfaces, as represented by aircraft blade detection, is still a challenge. Considering the narrow space between adjacent blades, the traditional spherical barrier boundary is not suitable for flat curved surface blades, which cannot obtain sufficient operational space. Furthermore, the lengths of obstacle avoidance paths in different directions vary greatly under the overall distortion characteristics of the blades, and HOCBF lacks explicit direction guidance. To navigate these challenges, we firstly propose an accurate surface envelope method with short solution time through rotated and scaled super-ellipsoids to obtain a large operational space. Building upon this, we propose a novel force-guided high-order control barrier function (FG-HOCBF) method to guide robot to closely adhere to the surface along the desired direction and complete detection of specific areas, which consists of two components: surface normal approach judgment and guiding force generation in desired direction. Finally, simulations and experiments validate the performance of the proposed method.**

I. Introduction

When a robot operates in a narrow environment with complex curved surfaces, such as aircraft engine blade detection, it is crucial to ensure that the robot does not collide with the surfaces [1],[2]. Due to the uncertainty of the surface detection area and the flexibility of the detection task, the obstacle avoidance method based on offline planning is not applicable in this scenario. For real-time obstacle avoidance method, artificial potential field (APF) method constructs the attractive field from the target point and the repulsive field from obstacles [3],[4]. However, in narrow environments, the repulsive fields can distort the original trajectory. High-order control barrier function (HOCBF) has been proposed recently to achieve safety control of high-order systems, which achieves the minimum modification of the nominal control torque by constructing a safety set based on distance constraints [5],[6]. Compared to APF, HOCBF does not modify the nominal control torque when moving away from the obstacle boundary, so it can better track the original trajectory to complete the detection task.

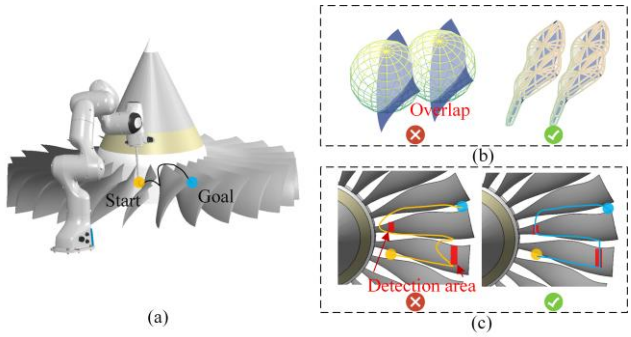

Fig. 1. Aircraft engine blades detection. (a)Scene. (b) The overlapping spherical safety boundary result in a small operational space. (c) Lack of direction guidance when avoiding obstacles may lead to task failure.

As an effective method for robots to avoid obstacle, HOCBF achieve strict safety control of robots by precisely characterizing the obstacle boundaries. For computational convenience, obstacles are often simply modeled as spheres [7],[8]. As shown in fig. 1, when performing surface detection tasks in narrow environments, due to the narrow space between adjacent surfaces, using a small number of large spheres can easily compress the operational space. Conversely, although a large number of small spheres can achieve a complete envelope, the computational cost is large. Therefore, it is necessary to precisely characterize the surface boundary to obtain a large operational space. Moreover, due to the regional difference of the curved surface, the lengths of the obstacle avoidance trajectories vary in different directions. Considering that the classical HOCBF method based on distance constraints will lead to the uncertainty in the avoidance direction, inappropriate avoidance directions can lead to redundant detour trajectories, and thus unable to approach the specific detection area. Therefore, the following challenges arise when performing close-range detection of specific area of curved surfaces in narrow environments.

The first challenge is how to precisely enclose complex surfaces in narrow environments to obtain a large operational space. Compared with spheres with a fixed shape, super-ellipsoids can change their shape by scaling semi-axis lengths. Since super-ellipsoids can also be explicitly parameterized, they have been widely used in object envelop [9]-[11]. The minimum volume enclosing super-ellipsoid (MVESE) method aims to minimize the volume of the super-ellipsoid to fitting the object point cloud [12],[13]. Although it achieves tight surface fitting, the parameter optimization process is complex. Neural networks method has proposed to envelope 3D objects that combines multiple super-ellipsoids [14],[15]. A loss function is defined based on bidirectional object reconstruction error, and the neural

*This work was supported by the National Natural Science Foundation of China under Grant 52322511, Grant 52188102, Grant 52575592.

Yujie Li, Fangyu Peng, Yukui Zhang, Rong Yan, Xiaowei Tang and Wenke Zhou are with the School of Mechanical Science and Engineering, Huazhong University of Science and Technology, Wuhan 430074, China. (e-mail: liyujie@hust.edu.cn, zwm8917@263.net, zhangyukui@hust.edu.cn, yanrong@hust.edu.cn, txwysxf@126.com, m202370637@hust.edu.cn).

Chen Chen is with Hubei Key Laboratory of Mechanical Transmission and Manufacturing Engineering, Wuhan University of Science and Technology, Wuhan, 430081, Hubei, China (e-mail: chenchen_1014@foxmail.com)

Zhitao Gao is with the School of Mechanical Science and Engineering, Huazhong University of Science and Technology, Wuhan 430074, China. (corresponding author, e-mail: gzt_1218@foxmail.com)

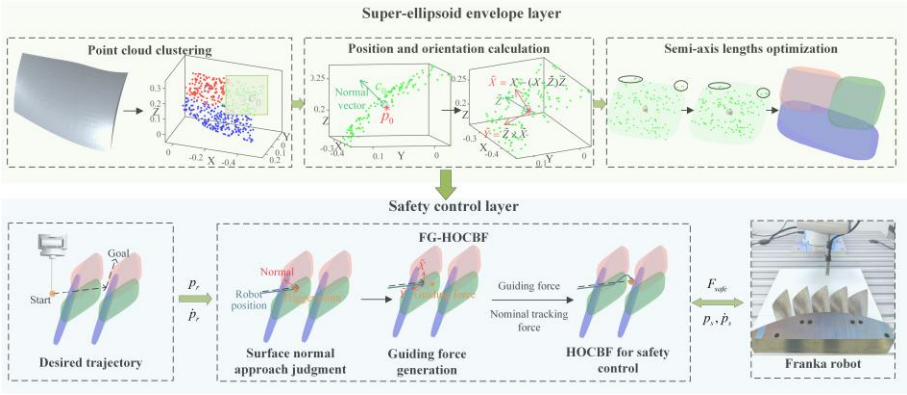

Fig. 2. The framework of proposed method, mainly consisting of the two parts: super-ellipsoid envelope layer and safety control layer.

network is trained to minimize it. The high training cost of this method limits its application in obstacle avoidance for robots.

The second challenge is how to effectively control the obstacle avoidance direction to obtain a short detour trajectory while performing close-range detection in the specific area. In [16], an augmented control barrier function (CBF) is constructed by adding a direction term to ensure positional space safety and an appropriate avoidance direction. Similarly, [17] generates safety control action by constructing multiple CBFs respectively for maintaining a safe distance and selecting an appropriate avoidance direction. However, these methods are only suitable for avoidance direction control in simple environments, and for complex obstacles in narrow environments, these methods may lead to infeasible solutions.

To address these challenges, we propose an accurate surface envelop method with short solution time that utilizes rotated and scaled super-ellipsoids to obtain a large operational space in narrow environments, and a force-guided high-order control barrier function (FG-HOCBF) method of obstacle avoidance in the desired direction. When the robot approaches the surface boundary roughly along the curved surface normal, a guiding force is generated in the desired direction, enabling the robot to adhere to the curved surface along the desired direction while accomplishing close-range detection in the specific area. The main contributions of this paper are as follows:

- A curved surface boundary characterization method that utilizes rotated and scaled super-ellipsoids has been proposed, which ensures a large operational space while reducing the solution time.
- A novel FG-HOCBF method is proposed to guide the robot to closely adhere to the surface along the desired direction and perform the close-range detection of the specific area.
- The effectiveness of the proposed method for surface detection in narrow environments has been verified.

II. Preliminaries and Framework Construction

A. High-Order Control Barrier Function

Consider a control affine system as

$$\dot{x} = f(x) + g(x)u\,, \tag{1}$$

where $x \in \mathbb{R}^n$ is the system state, $u \in \mathbb{R}^q$ is the control input, $f:\mathbb{R}^n \to \mathbb{R}^n$ is the drift term, and $g:\mathbb{R}^n \to \mathbb{R}^{n\times q}$ is the control influence term.

Definition 1: Assuming that system (1) is of relative degree m to its input u. A sequence of auxiliary functions is defined as

$$\begin{aligned} &\psi_0(x) = b(x) \\ &\psi_i(x) = \dot{\psi}_{i-1}(x) + \alpha_i(\psi_{i-1}(x)),\ 1 \le i \le m \end{aligned}, \tag{2}$$

where $b:\mathbb{R}^n \to \mathbb{R}$ is a constraint function that satisfies $b(x) \ge 0$, $\alpha_i(\cdot)$ is sufficiently smooth class $\mathcal{K}$ functions. The associated sets are

$$C_i = \{x \in \mathbb{R}^n : \psi_{i-1}(x) \ge 0\},\ 1 \le i \le m\,. \tag{3}$$

Definition 2: (High-order control barrier function [5]) Let $\psi_1(x),...,\psi_m(x)$ be defined by (2) and $C_1,...,C_m$ be defined by (3). The function b is a HOCBF of relative degree m for system (1) if there exist class $\mathcal{K}$ functions α_i, $i \in \{1,...,m\}$, such that

$$\begin{aligned} &\sup_{u\in U}[\mathcal{L}_f^m b(x) + \mathcal{L}_g\mathcal{L}_f^{m-1}b(x)u + O(b(x)) \\ &+\alpha_m(\psi_{m-1}(x))] \ge 0,\ \forall x \in C_1 \cap,...,\cap C_m \end{aligned}, \tag{4}$$

or in a simpler form $\psi_m(x) \ge 0$.

Given an HOCBF $b(x)$ with the associated sets $C_1,...,C_m$ defined by (3), if $x(t_0) \in C_1(t_0) \cap,...,\cap C_m(t_0)$, then any input u that satisfies the constraint in (4), $\forall t \ge 0$ renders $C_1 \cap,...,\cap C_m$ forward invariant for system (1).

B. Statement and Framework Construction

When performing the curved surface detection task in a narrow environment composed of complex surfaces, it is necessary to accurately characterize the surface boundary to obtain a large operational space. Moreover, due to the large difference in the regional characteristics of surfaces although HOCBF based on distance constraints can ensure safety, it will lead to the uncertainty of avoidance direction and thus obtain redundant detour trajectories.

As shown in Fig. 2, to address the aforementioned challenges, a framework mainly consisting of two components has been constructed:

1) Surface envelope layer: This layer proposes a method that utilizes rotated and scaled super-ellipsoids to envelop curved surfaces for a large operational space. The point cloud clustering, projection and optimization algorithms are introduced to obtain the center position, orientation and semi-axis lengths of the super-ellipsoid, respectively.

2) Safety control layer: This layer proposes FG-HOCBF to control the avoidance direction and perform close-range surface detection of the specific area. Firstly, the surface normal approach judgment module judges the robot behavior of approaching the surface boundary. Then, guiding force generation in desired direction module guides robot to closely adhere to the surface along the desired direction and perform detection of specific areas. Finally, the guiding force and nominal tracking force are combined as a new nominal control force, which is minimally modified by the HOCBF to strictly ensure safety.

III. Rotated and Scaled Super-Ellipsoids Envelope for a Large Operational Space

This section introduces an accurate curved surface boundary characterization method with short solution time that utilizes rotated and scaled super-ellipsoids. The envelope region of a single super-ellipsoid is obtained by partitioning the point cloud.

A. Surface Partitioning Based on Point Cloud Clustering

Due to varying curvatures and different normal directions across the curved surface, partitioning point cloud with similar normal and close proximity into the same cluster helps reduce the volume of super-ellipsoids required for the envelope surface. K-means clustering, as one of the most commonly used unsupervised learning algorithms in point cloud data processing, aims to partition the point cloud data into K compact and well-separated clusters through iterative optimization [18]. The traditional K-means clustering algorithm based only on Euclidean distance may cause point cloud with large curvature variations to be wrongly classified into the same cluster, resulting in a large volume of super-ellipsoid required for subsequent envelope. Thus, we improve the traditional K-means clustering algorithm as

$$D_{il} = \alpha \frac{\arccos(n_i \cdot \bar{n}^{(l)})}{\arccos(n_i \cdot \bar{n}^{(l)})_{\max}} + (1-\alpha) \frac{\left\| p_i - \bar{p}^{(l)} \right\|}{\left\| p_i - \bar{p}^{(l)} \right\|_{\max}}, \quad (5)$$

$$\bar{p}^{(l)} = \frac{\sum_{i \in G_l} p_i}{m_l},\ \bar{n}^{(l)} = \frac{\sum_{i \in G_l} n_i}{m_l}, i = 1,2,...,m,\ l = 1,...,k, \quad (6)$$

where D_{il} is the distance from the i^{th} point to the center of the l^{th} cluster. $\bar{p}^{(l)}$ and $\bar{n}^{(l)}$ are the center position and normal of the l^{th} cluster, respectively. $\alpha \in [0,1]$ is weighting factor of the cosine similarity. p_i and n_i are the position and normal of the i^{th} point, respectively. m is the number of points in the point cloud and k is the number of clusters. m_l is the number of points in the l^{th} cluster.

Remark 1: The smaller α is, the less influence the difference in normality has on point cloud clustering. A genetic optimization algorithm is employed to determine the optimal value of α, resulting in the minimal total volume of the super-ellipsoids [19].

After obtaining the distance from the i^{th} point to the center of the l^{th} cluster using (5), we classify the i^{th} point into the cluster with the closest distance. Then, we recalculate the center position and normal of each cluster of point cloud using (6), and re-cluster using (5) until the center position and normal of each cluster no longer change.

B. Center Position and Orientation Calculation

After point cloud clustering is completed, we enclose the clustered point cloud with super-ellipsoids. The standard equation of a super-ellipsoid can be written as [9]

$$\left(\frac{x-x_0}{a}\right)^{2n} + \left(\frac{y-y_0}{b}\right)^{2n} + \left(\frac{z-z_0}{c}\right)^{2n} = 1, \quad (7)$$

where $[x_0\ y_0\ z_0]^T$ represents the center point, $[x\ y\ z]^T$ represents a generic point, a, b, c represent the semi-axis lengths of the super-ellipsoid, and $n \geq 2$ is the shape parameter. A super-ellipsoid perfectly approximates a cuboid as the shape parameter approaches infinity, as shown in fig. 3.

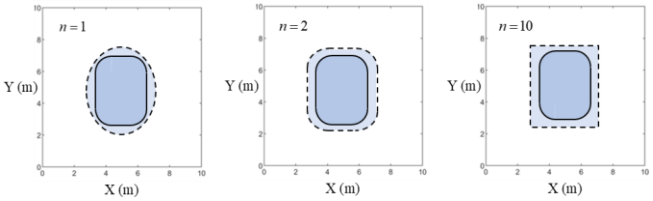

Fig. 3. The influence of shape parameter on the shape of a superellipsoid.

The super-ellipsoid in the general pose can be expressed in matrix form as

$$\left[\left|R^T(p-p_0)\right|^n\right]^T A \left[\left|R^T(p-p_0)\right|^n\right] = 1, \quad (8)$$

where p_0 is the center position of the super-ellipsoid where $R \in \mathbb{R}^{3\times3}$ is the orientation matrix of the super-ellipsoid and $A \in \mathbb{R}^{3\times3}$ is the diagonal matrix that describes the semi-axis lengths of the super-ellipsoid. Therefore, in order to obtain an appropriate super-ellipsoid, we must know its center position and orientation as well as its semi-axis lengths.

In order to obtain the center position of the super-ellipsoid, the point closest to the center of the point cloud is identified and the point is moved approximately half the surface thickness in the opposite normal direction to obtain the center position

$$p_0 = c_0 - \frac{t}{2}((n_0)^T I_3), \quad (9)$$

where c_0 and n_0 are the center and normal of the cluster. t is the surface thickness and $I_3 \in \mathbb{R}^{3x3}$ is an identity matrix.

In order to obtain the orientation of the super-ellipsoid, the normal of the cluster is regarded as the $\tilde{Z}$ axis of the super-ellipsoid firstly. If the overall extent of the point cloud along the X-axis of the world coordinate system is greater than

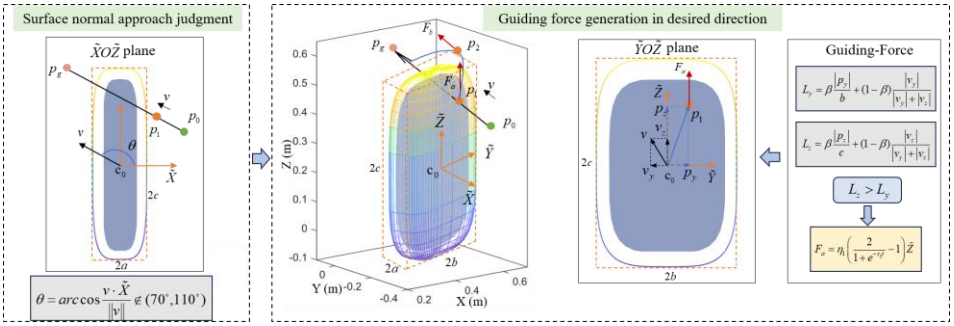

Fig. 4. Schematic diagram of FG-HOCBF. When the angle θ between the velocity v and the shortest semi-axis direction $\tilde{X}$ satisfies $\theta \notin (70°,110°)$, robot needs to bypass the surface boundary along the desired direction. The guiding force direction F_a is determined comprehensively by the position projection and the velocity ratio of the intersection point p_1 on the super-ellipsoid. The guiding force F_b is generated at point p_2 after F_a disappears.

that along the Y-axis, the X-axis is projected onto the plane perpendicular to the normal to obtain the $\tilde{X}$ axis of the super-ellipsoid. The $\tilde{Y}$ axis is then derived via the cross product of the vectors

$$\tilde{X} = \frac{X - (X \cdot \tilde{Z})\tilde{Z}}{\left\| X - (X \cdot \tilde{Z})\tilde{Z} \right\|}, \tag{10}$$

$$\tilde{Y} = \tilde{Z} \times \tilde{X}, \tag{11}$$

$$R = [\tilde{X}; \tilde{Y}; \tilde{Z}], \tag{12}$$

where R is the orientation of the super-ellipsoid.

C. Semi-Axis Lengths Optimization

To fully enclose the partitioned point cloud, the semi-axis lengths optimization algorithm is proposed. After calculating the range of each cluster of point cloud along each axis of the world coordinate system, the initial semi-axis lengths a_0, b_0 of the super-ellipsoid along the $\tilde{X}$ axis and $\tilde{Y}$ axis are obtained through the Pythagorean theorem [20]. The semi-axis length c of the $\tilde{Z}$ axis can be directly set to the calculated value of the surface thickness multiplied by a scaling factor.

To obtain the optimized semi-axis lengths, the outermost point p_{out} located outside the super-ellipsoid in the point cloud based on the initial semi-axis length is identified. Then, the optimized semi-axis lengths a, b can be calculated as

$$\begin{cases} a = \sigma_x \cdot a_0, & \text{if } \overrightarrow{p_{out}p_0} \cdot \tilde{X} \geq \overrightarrow{p_{out}p_0} \cdot \tilde{Y} \\ b = \sigma_y \cdot b_0, & \text{otherwise} \end{cases}, \tag{13}$$

$$\sigma_i = \sigma_i + \rho,\ i = x,\ y, \tag{14}$$

where $\overrightarrow{p_{out}p_0}$ is the vector from the center of super-ellipsoid to the outermost point. σ_x and σ_y are scaling factors along the $\tilde{X}$ axis and $\tilde{Y}$ axis, both increasing with the gain of ρ.

IV. FG-HOCBF for Close-Range Detection of Specific Curved Surfaces Area

After characterizing the surface boundary using super-ellipsoids, due to the large regional difference of the curved surface, the classical HOCBF based on distance constraints leads to an uncertain avoidance direction. Inspired by magnetic field force-guided obstacle avoidance [21], we propose the FG-HOCBF method to control the avoidance direction and perform close-range surface detection of specific area. The main steps of FG-HOCBF are shown in fig. 4.

A. Surface Normal Approach Judgment

The judgment function $\sigma(p)$ is constructed as:

$$\sigma(p) = \left[\left| R^T (p - p_0) \right|^n \right]^T A \left[\left| R^T (p - p_0) \right|^n \right] - 1, \tag{15}$$

$$A = diag\{\frac{1}{a^{2n}}, \frac{1}{b^{2n}}, \frac{1}{c^{2n}}\}, \tag{16}$$

considering a certain safety margin, the original shortest semi-axis length is enlarged by 0.5 times, while the remaining semi-axes lengths are enlarged by 0.2 times.

When $\sigma(p) = 0$, the reference trajectory intersects with the super-ellipsoid constructed by the judgment function at point p_1. Then the angle of the θ is used to determine whether to consider the avoidance direction

$$\theta = arc\cos\frac{v_1 \cdot \tilde{S}}{\|v_1\|}, \tag{17}$$

Where v_1 is the velocity at the intersection point p_1, and $\tilde{S}$ is the shortest semi-axis direction and can be approximately regarded as the surface normal.

Remark 2: When $\theta \notin (70°,110°)$ is satisfied, it means that the reference trajectory approaches the surface roughly along the surface normal. In this case, it is necessary to consider bypassing the surface boundary along the desired direction via the shortest detour path.

B. Guiding Force Generation in Desired Direction

When the robot needs to bypass the surface boundary, the desired avoidance direction at the end effector is determined comprehensively by using the position projection and the velocity ratio of the intersection point p_1 on the super-ellipsoid

$$L_i = \beta \frac{\left|\overrightarrow{p_0 p_1} \cdot R_i\right|}{\eta_i} + (1-\beta)\frac{|v_{1i}|}{\sum|v_{1i}|},\ i = 1,\ 2,\ 3, \quad (18)$$

where $\beta \in (0,1)$ is the weighting factor, R_i is the i^{th} column of the orientation matrix, η_i is the i^{th} semi-axis length, and v_{1i} is the i^{th} component of the velocity vector in the super-ellipsoid coordinate system. The maximum value of L_i is calculated, in which case the semi-axis direction corresponding to index i is the desired avoidance direction.

The magnitude of the guiding force is calculated in sigmoid form as

$$F_i = \eta_i \left(\frac{2}{1+e^{-\tau t_i}} - 1 \right),\ i = a,\ b, \quad (19)$$

where F_i is the guiding force, η_i is the maximum value of F_i. Through the sigmoid function, F_i is gradually increased from 0 to η_i. τ is the growth rate of the guiding force, and t_i is the duration time.

The guiding force F_a is generated at the intersection point p_1 firstly. Under the influence of this guiding force, the robot end-effector moves a certain distance along the desired direction to reach point p_2. After the guiding force F_a disappears, the end-effector may return to the trajectory generated by HOCBF alone. Therefore, another guiding force F_b is generated at the point p_2 along the direction of the reference trajectory velocity v_2.

Remark 3: The guiding force F_a is generated only once to prevent trajectory oscillation, and the duration is from $\sigma(p_1) = 0$ to $\sigma(p_2) > 0$. After the guiding force F_a disappears, the guiding force F_b is generated and the duration is fixed at one second.

C. HOCBF for Safety Control

We use a nominal PD controller to trace the reference trajectory

$$F_{no} = K(p_r - p_s) + D(\dot{p}_r - \dot{p}_s), \quad (20)$$

where p_r and p_s are reference trajectory and robot safe trajectory, respectively. K and D are stiffness and damping matrices of the nominal controller.

When the robot approaches the surface boundary, the guiding force mentioned above works together with the tracking force generated by the PD controller as the new nominal tracking force $F_{no}^{'}$. The safe control force F_{safe} is derived by modifying the new nominal force $F_{no}^{'}$ through solving a quadratic program

$$\begin{aligned} F_{safe} &= \arg\min_{F \in \mathbb{R}^q} \frac{1}{2}\left\| F - F_{no}^{'} \right\| \\ s.t. \mathcal{L}_f^2 h(x) + \mathcal{L}_g \mathcal{L}_f h(x) F + (\alpha_1 + \alpha_2)\dot{h}(x) + \alpha_1 \alpha_2 h(x) &\geq 0 \end{aligned} \quad .(21)$$

V. Simulation Studies

Two simulation studies are carried out to verify the proposed method, including: comparison of surface envelope methods (Simulation 1), effectiveness of the FG-HOCBF for close-range surface detection in the desired direction (Simulation 2). The simulation is Matlab/Simulink, and the details can be found in the attached video.

A. Simulation 1: Comparison of Surface Envelope Methods

By using the proposed method that utilizes rotated and scaled super-ellipsoid to envelop curved surface, we have successfully achieved an accurate envelope from simple to complex surfaces, as shown in Fig. 5.

We use the total volume of the super-ellipsoids to indirectly measure the size of the operational space. The total volume and solution time for enveloping surfaces using spheres, the MVESE method, and the proposed method are shown in Fig. 6. Compared to sphere-based envelope surface, the proposed method occupies a smaller volume in the space while fully enveloping the surface, thereby providing a larger operational space for the robot. In contrast to the MVESE method, the proposed method takes into account the normal angle difference during point cloud clustering, which can further reduce the total envelope volume. At the same time, it only considers the semi-axis length optimization, achieving a shorter solution time. The total volume and solution time of the proposed method are $0.00115\ m^3$ and $1.74\ s$, compared to the MVSEE method ($0.00125\ m^3$ and $3.78\ s$).

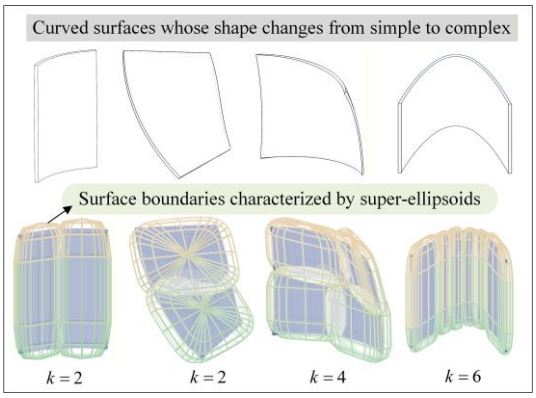

Fig. 5. Different numbers of super-ellipsoids are used to enclose curved surfaces with shapes changing from simple to complex.

Method	Sphere envelope	MVSEE method	Proposed method
	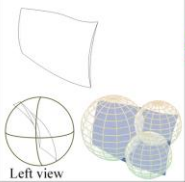	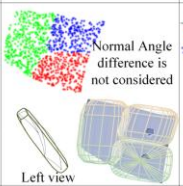	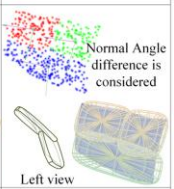
Total volume (m^3)	0.0428	0.00125	0.00115
Solution time (s)	0.028	3.78	1.74

Fig. 6. Comparison of the total volume and solution time of the three envelope methods. When performing point cloud clustering, MVSEE does not consider the normal angle difference, while proposed method does.

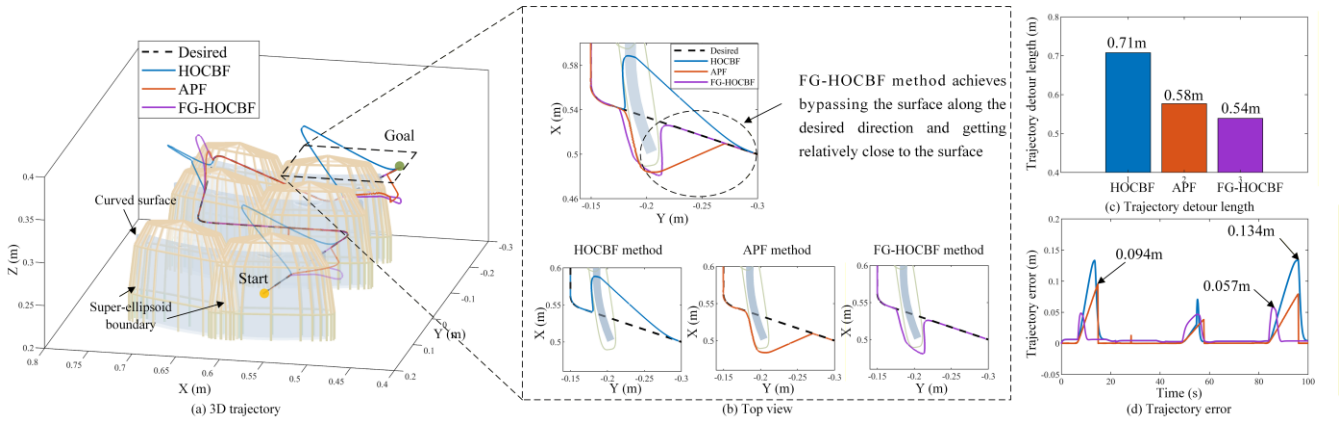

Fig. 7. Trajectory comparison for simulation 2. (a) 3D trajectory. (b) Top view. The area circled can be seen directly that FG-HOCBF method achieves bypassing the surface along the desired direction and getting relatively close to the surface. (c) Trajectory detour length. (d) Trajectory error.

B. *Simulation 2: Effectiveness of the FG-HOCBF for Close-Range Surface Detection in the Desired Direction*

Simulations 2 test the effectiveness of the FG-HOCBF for close-range surface detection in the desired direction. The robot used in the simulation is Franka robot whose model parameters are taken from [22]. The virtual robot needs to track a reference trajectory smoothly spliced together by five linear trajectories from start point $p_0 = [0.55, 0.2, 0.28]$ m to goal point $p_g = [0.5, -0.3, 0.28]$ m .The workspace contains three small curvature surface obstacles of the same shape, with the distances between adjacent surfaces being 0.2 m and 0.1 m respectively. Each surface is enveloped by two super-ellipsoids whose parameters are obtained by the rotated and scaled super-ellipsoid method. The simulation carries out a comparison of the obstacle avoidance performance using three methods: the classical HOCBF, APF and proposed FG-HOCBF methods.

As shown in Fig. 7, the classical HOCBF method, consistently bypasses the surface boundary in the same direction. When approaching the joint limits, it may fail to complete the task. The APF method achieves obstacle avoidance in the expected direction, but fails to promptly track the reference trajectory after obstacle avoidance. In contrast, the proposed FG-HOCBF method, achieves bypassing the surface in the desired direction and getting relatively close to the surface. As shown in Fig. 7(c), the detour trajectory length of the proposed method is 0.057 m, compared to the HOCBF (0.134 m) and the APF (0.094 m) methods, respectively. As shown in Fig. 7(d), the maximum trajectory error of the proposed method is 0.057 m, achieving error reductions of 57.5% compared to the classical HOCBF (0.134 m) and 39.4% compared to the APF (0.094 m) methods, respectively.

VI. Experimental Results

We further carry out a real-world aircraft engine blade model detection experiment to verify the comprehensive performance of the proposed FG-HOCBF method. The experimental setup is shown in Fig. 8, which mainly includes the Franka robot and the industrial endoscope at its end for detection. The Franka end posture is kept vertical to the plane of the platform during the experiments. The task requires the robot to perform the detection of three blades.

After enveloping the blade surfaces with super-ellipsoids, the obstacle avoidance performance of the three methods is compared: the classical HOCBF, the APF and the proposed FG-HOCBF methods. The global experimental trajectories are shown in Fig. 9(a). Compared with the classical HOCBF and APF methods, the proposed FG-HOCBF method achieves bypassing the surface in the desired direction, and getting relatively close to the surface. As shown in Fig. 9(e), the detour trajectory length of the proposed method is 0.18 m, compared to the classical HOCBF (0.21 m) and APF (0.27 m) methods, respectively.

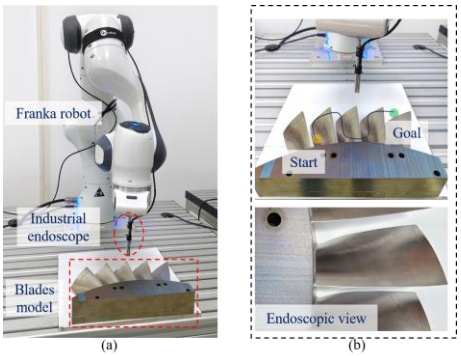

Fig. 8. (a) experiment setup. (b) Detaile view and endoscope view.

VII. Conclusion

To achieve close-range detection of specific curved surfaces area in narrow environments，such as aircraft engine blade detection, we propose a FG-HOCBF method to guide robot to bypass the surface in the desired direction and get relatively close to the surface. Firstly, to achieve a larger operational space, we proposed an accurate envelop method with short solution time that utilizes rotated and scaled super-ellipsoids. On this basis, the FG-HOCBF method is proposed to achieve the desired avoidance direction and close-range detection of specific surface area. Simulations and experiments show that, compared with the spherical envelope and MVESE methods, the proposed envelope method can obtain a large operational space and short solution time. Compared with HOCBF and APF, the proposed FG-HOCBF guides robot to bypass the surface in the desired direction with the shortest detour trajectory length while achieving the close-range detection of specific curved surfaces area.

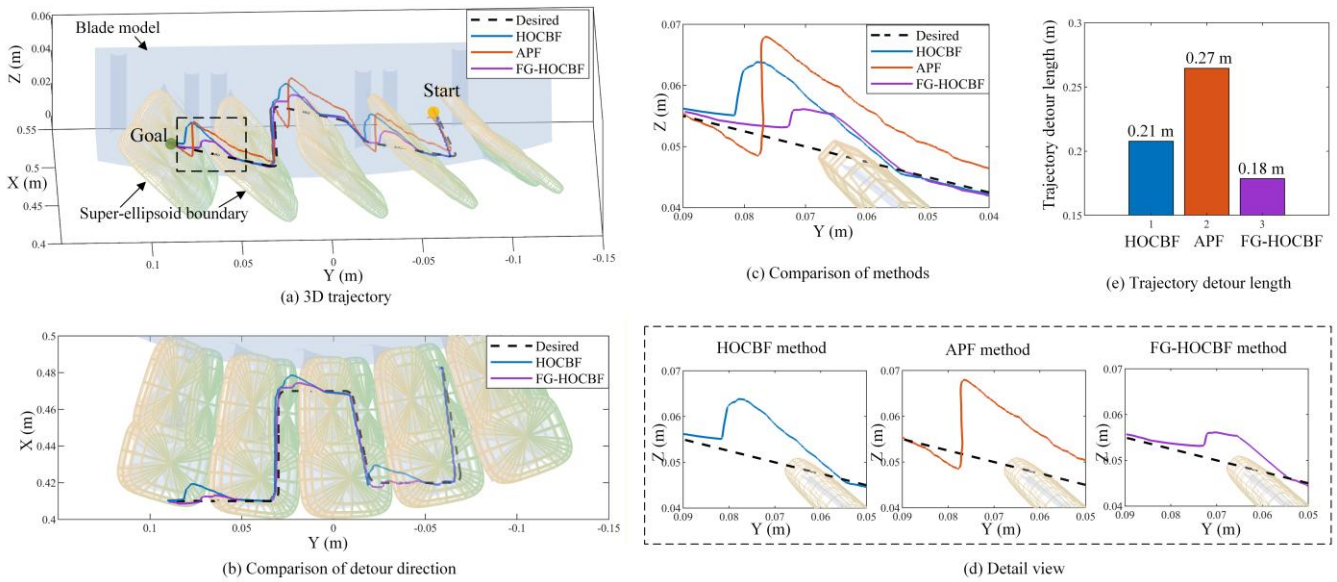

Fig. 9. Trajectory comparison for aircraft engine blade model detection experiment. (a) 3D trajectory. (b) Comparison of detour direction. (c) Comparison of methods. (d) Detail view. (e) Trajectory detour length.

REFERENCES

[1] Y. Wang *et al.*, "An aero-engine inspection continuum robot with tactile sensor based on EIT for exploration and navigation in unknown environment," in *2019 IEEE/ASME International Conference on Advanced Intelligent Mechatronics (AIM)*, Jul. 2019, pp. 1157–1162.

[2] J. Duan, B. Wang, K. Cui, and Z. Dai, "Path Planning Based on NURBS for Hyper-Redundant Manipulator Used in Narrow Space," *Applied Sciences*, vol. 12, no. 3, p. 1314, Jan. 2022.

[3] Z. Pan, C. Zhang, Y. Xia, H. Xiong, and X. Shao, "An Improved Artificial Potential Field Method for Path Planning and Formation Control of the Multi-UAV Systems," *IEEE Transactions on Circuits and Systems II: Express Briefs*, vol. 69, no. 3, pp. 1129–1133, Mar. 2022.

[4] A. Gottardi, S. Tortora, E. Tosello, and E. Menegatti, "Shared Control in Robot Teleoperation With Improved Potential Fields," IEEE Trans. Human-Mach. Syst., vol. 52, no. 3, pp. 410–422, Jun. 2022.

[5] W. Xiao and C. Belta, "High-Order Control Barrier Functions," IEEE Transactions on Automatic Control, vol. 67, no. 7, pp. 3655–3662, Jul. 2022.

[6] W. Xiao and C. Belta, "Control Barrier Functions for Systems with High Relative Degree," Mar. 13, 2019, arXiv:1903.04706.

[7] J. Liu et al., "Flexible Active Safety Motion Control for Robotic Obstacle Avoidance: A CBF-Guided MPC Approach," IEEE Robotics and Automation Letters, vol. 10, no. 3, pp. 2686–2693, Mar. 2025.

[8] J. Lin, D.-H. Zhai, Y. Xiong, and Y. Xia, "Safety Control for UR-Type Robotic Manipulators via High-Order Control Barrier Functions and Analytical Inverse Kinematics," *IEEE Transactions on Industrial Electronics*, vol. 71, no. 6, pp. 6150–6160, Jun. 2024.

[9] A. H. Barr, "Superquadrics and Angle-Preserving Transformations," *IEEE Computer Graphics and Applications*, vol. 1, no. 1, pp. 11–23, Jan. 1981.

[10] F. Jaillet, "Segmentation and Superquadric Modeling of 3D Objects." International Conference in Central Europe on Computer Graphics and Visualization, 2003.

[11] H. Wu, Y. Liu, C. Wang, and Y. Wei, "Global Semantic Localization from Abstract Ellipse-Ellipsoid Model and Object-Level Instance Topology," Remote Sensing, vol. 16, no. 22, Art. no. 22, Jan. 2024.

[12] R. Shioda and L. Tunçel, "Clustering via minimum volume ellipsoids," Computational Optimization and Applications, vol. 37, no. 3, pp. 247–295, Jun. 2007.

[13] S. Ruan, K. L. Poblete, H. Wu, Q. Ma, and G. S. Chirikjian, "Efficient Path Planning in Narrow Passages for Robots With Ellipsoidal Components," IEEE Transactions on Robotics, vol. 39, no. 1, pp. 110–127, Feb. 2023.

[14] D. Paschalidou, A. O. Ulusoy, and A. Geiger, "Superquadrics Revisited: Learning 3D Shape Parsing Beyond Cuboids," in *2019 IEEE/CVF Conference on Computer Vision and Pattern Recognition (CVPR)*, Jun. 2019, pp. 10336–10345.

[15] D. Paschalidou, L. Van Gool, and A. Geiger, "Learning Unsupervised Hierarchical Part Decomposition of 3D Objects From a Single RGB Image," in 2020 IEEE/CVF Conference on Computer Vision and Pattern Recognition (CVPR), Jun. 2020, pp. 1057–1067.

[16] G. Wu and K. Sreenath, "Safety-critical control of a planar quadrotor," in *2016 American Control Conference (ACC)*, Boston, MA, USA: IEEE, Jul. 2016, pp. 2252–2258.

[17] S. H. Khan and A. Ghaffari, "Multi-Objective Trajectory Planning for Unmanned Aerial Vehicles Using CLF-CBF-Based Quadratic Programs," in *2023 American Control Conference (ACC)*, San Diego, CA, USA: IEEE, May 2023, pp. 726–731.

[18] A. Mahdaoui and E. H. Sbai, "3D Point Cloud Simplification Based on k-Nearest Neighbor and Clustering," Advances in Multimedia, vol. 2020, no. 1, p. 8825205, 2020.

[19] S. Katoch, S. S. Chauhan, and V. Kumar, "A review on genetic algorithm: past, present, and future," Multimed Tools Appl, vol. 80, no. 5, pp. 8091–8126, Feb. 2021.

[20] R. V. Kadison, "The Pythagorean Theorem: I. The finite case," Proceedings of the National Academy of Sciences, vol. 99, no. 7, pp. 4178–4184, Apr. 2002.

[21] A. Ataka, H.-K. Lam, and K. Althoefer, "Magnetic-Field-Inspired Navigation for Robots in Complex and Unknown Environments," Front. Robot. AI, vol. 9, p. 834177, Feb. 2022.

[22] C. Gaz et al., "Dynamic identification of the Franka Emika Panda robot with retrieval of feasible parameters using penalty-based optimization," *IEEE Robot. Autom. Lett.*, vol. 4, no. 4, pp. 4147–4154, Oct. 2019.